ECS Transactions, 42 (1) 3-22 (2012)
10.1149/1.4705474 ©The Electrochemical Society

Electrochemistry of The Nickel Electrode as a Cathode Catalyst In The Media Of Acidic Peroxide For Application of The Peroxide Fuel Cell

Ayşe Elif SANLI[a], Aylin AYTAÇ[b]

[a] Turgut Özal University, Engineering Faculty, Electrical and Electronics Engineering Faculty, Ankara, TURKEY
[b] Gazi University, Faculty of Science, Department of Chemistry, Ankara, TURKEY

Hydrogen peroxide reduces on the nickel electrode surface in the acidic medium. On the nickel electrode the passive film layers such as NiS and NiOOH form in the peroxide free solution. However the nickel surface was activated with the addition of the peroxide. The cyclic voltammetry (CV) and impedance (EIS) studies verified the passivation and activation states in peroxide free acidic solution and the acidic peroxide solution. The electrochemical reactions of the sulphuric acid and peroxide at nickel electrode were electrochemically analyzed by cyclic voltammetry (CV) and impedance spectroscopy (EIS)

Introduction

The biggest disadvantage of PEM fuel cells is the hydrogen storage so the related research is focused on developing new kinds of fuel cells and producing new hydrogen storage materials. $NaBH_4$ is a good alternative as hydrogen storage material because of its protide (H^-) content. Also $NaBH_4$ is being used as a direct fuel in direct borohydride/peroxide fuel cells (DBPFCs). The cell potential of borohydride/peroxide fuel cells can be increased up to 2.11 V with the use of suitable anode and cathode material. This potential is much higher than that obtainable with PEM fuel cells. The cell reactions are as follows:

Anode reaction:	$BH_4^- + 2H_2O \rightarrow BO_2 + 8H^+ + 8e^-$	$E^0 = -0.476$ V
Cathode reaction:	$4H_2O_2 + 8H^+ + 8e^- \rightarrow 8H_2O$	$E^0 = 1.776$ V
Total cell reaction:	$NaBH_4 + 4H_2O_2 \rightarrow NaBO_2 + 6H_2O$	$E^0 = 2.1$ V

There are a few studies to develop the new anode and cathode materials for DBPFCs (1-3). Among these is the silver electrode used as anode and it was found that catalytic silver oxides promote the $6e^-$ transfer oxidation of $NaBH_4$ (4-6).

The oxidant generally used in fuel cells is oxygen or air. However the reduction of oxygen is the prime cause of the loss of polarization in the cells. It is known that the use of a liquid oxidant such as H_2O_2 decreases both the oxygen activation and concentration overvoltages and obviates most of the problems encountered due to the presence of oxygen (7). Handling, storage and feeding of hydrogen peroxide, a liquid oxidant, to a fuel cell are easier than a gas phase oxidant. The use liquid oxidant gives a two phase reaction while the use of oxygen results the addition of an another phase. The fuel cell operates much more steadily in two-phase system than operating in three-phase system.

Downloaded on 2017-10-16 to IP 54.70.40.11 address. Redistribution subject to ECS terms of use (see ecsdl.org/site/terms_use) unless CC License in place (see abstract).

Leon et.al report that the use of H_2O_2 as an oxidant instead of the air has a positive effect on the performance of the DBFCs (8).

Different types of electrocatalysts for hydrogen peroxide reduction have been reported (9-13). They are mainly noble metals such as platinum, palladium, iridium, silver, gold, and carbon-supported Prussian Blue (PB) as mediated electron-transfer cathode catalyst. Using Pourbaix diagrams, gold (Au/C) was identified as an effective catalyst, which minimizes gas evolution and provides high power density with the use of hydrogen peroxide (11). However there is an urgent need for the development of catalysts using cost effective materials due extensive prices of the noble metals.

Nickel is one of the most important industrial metals and is used in a large number of applications. The behavior of the Ni in strongly acidic solutions (H_2SO_4, pH 1.0), has been extensively studied (12-15). It's reported that a passivating film forms on the nickel electrode in the acidic solution. The addition of H_2O_2 into the acidic media changes the potentiodynamic behavior of Ni significantly. Du et.al investigated the role of H_2O_2 in the oxide formation and the ionic dissolution of nickel using electrochemical methods. It was observed that the cathodic reduction of H_2O_2 predominated over the anodic dissolution of Ni. In contrast to the passivation behavior of Ni in peroxide-free solution, Ni shows an active dissolution in solutions containing H_2O_2 (12).

Experimental impedance data are usually interpreted using appropriate models and the related parameters are obtained by fitting the data into the simulated impedance spectra. Depending on the model, the parameters can be attributed physical or chemical meanings or remain a purely empirical description of the system. There are two different model concepts: 1) Electrical models in the form of equivalent circuits representing physical and/or chemical processes and 2) Physicochemical model in the form of a microkinetic description of chemical reactions, charge-transfer reactions and diffusion processes.

This paper presents and compares two methods of calculating reaction parameters such as the rate and diffusion constants based on CV and EIS data. The equivalent circuit was modeled by software provide by CHI potansiyostat/galvanostat.

In order to clarify the role of nickel as a cathode catalyst in the borohydride/peroxide fuel cell we studied the electrochemical behavior of nickel electrode in the acidic and the acidic+peroxide media by the use of electrochemical techniques such as CV and EIS.

Experimental

All experiments were carried out with CHI Instrument potansiostat /galvanostat. Ni net (100 mesh) sized 3x2 mm^2 was used as a working electrode. Pt wire from BAS and SCE from BASS were used as the counter and the reference electrodes.

CV Studies

Electrochemical were carried out in 0.1M H_2SO_4 solution and contained different amounts of 1 M H_2O_2 solution (1- 6 ml) in 10 ml 0.1 M H_2SO_4. Cyclic voltammograms were taken at the scan rate of 50 mV/s and the potential range of 0.8 V/ -0.8 V.

Downloaded on 2017-10-16 to IP 54.70.40.11 address. Redistribution subject to ECS terms of use (see ecsdl.org/site/terms_use) unless CC License in place (see abstract).

Physical characterization studies

The particle structures of the oxides formed on Nickel electrode and the morphology of the coated electrode were examined by Philips XL30 SFEG Energy dispersive X-ray spectroscopy (EDAX) and Scanning Electron Microscopy (SEM), respectively.

Electrochemical Impedance studies

The impedance data were recorded in the frequency range between 100 kHz and 10 mHz using CHI potansiyostat/galvanostat as an electrochemical impedance analyzer. An ac signal of 10 mV was applied potantiostatically at open-circuit condition. The results were displayed as Nyquist plots. Equivalent circuits were simulated by the use of the CHI Instrument software.

Result and Discussions

Behavior of the Ni electrode in the acidic medium

There are so many studies on the passivation of nickel in different acidic solutions (14-16). Figure 1 shows multi-cycle voltammograms for Nickel in H_2SO_4 solution. In this figure current-/voltage curves show the characteristic passivation behavior, i.e. an initial increase of the anodic current density due to active metal dissolution followed by a sudden drop of the current density corresponding to passive layer formation. There were three oxidation peaks located at the zero point potential (peak I), 0.35 V (peak II) and 0.45 V (peak III) observed in the multi-cyle CV graph.

i. Peak I does not change with cycling. The appearance of the peak at 0.0 V should be due to reaction [1], where the surface is covered by $(NiOH)_{ads}$ as the first step of the dissolution of the Ni . Then the anodic dissolution mechanism of Ni in acidic solution may occur according to the following reactions [12]:

$$Ni + H_2O \rightarrow (NiOH)_{ads} + H^+ + e^- \quad (1)$$

$$(NiOH)_{ads} \rightarrow Ni(OH^+)_{ads} + e^- \quad (2)$$

$$Ni(OH^+)_{ads} + H_2O \rightarrow Ni(OH)_2 + H^+ \quad (3)$$

$$Ni(OH)_2 + 2H^+ \rightarrow Ni^{+2} + 2H_2O \quad (4)$$

$$Ni(OH)_2 \rightarrow NiO(Ni_2O_3) \quad (5)$$

$$\text{Net reaction: } Ni \rightarrow Ni^{+2} + 2e^- \quad (6)$$

ii. Peak II shows a decrease of the potential and current related to the formation of a stable nickel sulphide layer (reactions 7-8). Cyclic voltammetry of Ni in H_2SO_4 gives an irreversible peak at the potential of 0.15 V which corresponds closely to the potential where Ni salt appears to be stable. At this potential, the reduction reaction of H_2SO_4 is assumed to involve the reduction of sulphuric acid to the S^{-2} species. This must be the process responsible for the growth of the nickel salt layer according to the following reaction (17):

Downloaded on 2017-10-16 to IP 54.70.40.11 address. Redistribution subject to ECS terms of use (see ecsdl.org/site/terms_use) unless CC License in place (see abstract).

$$H_2SO_4 + 8e^- + 8H^+ \rightarrow H_2S + 4H_2O \quad [7]$$

$$Ni^{+2} + H_2S \rightarrow NiS + 2H^+ \quad [8]$$

iii. Peak III was attributed to the formation of a passive NiOOH oxide film and the reduction of H_2SO_4. Corresponding reaction would be:

$$H_2SO_4 + 6e^- + 6H^+ \rightarrow S + 4H_2O \quad [9]$$

$$Ni + H_2SO_4 \rightarrow NiOOH + SO_2 + H^+ + e^- \quad [10]$$

Passivation took place on the electrode surface as observed in Figure 1. The fact that both peak currents and the peak potentials fall with the scan indicates the formation of passive films on Nickel surface. The passive films in sulfuric acid solution could be NiOOH (reaction 10) or NiO and Ni_2O_3 (14-16). As seen Figure 2, in addition to the CV scans the passivation is also clearly apparent in Nyquist diagrams which exhibit the inductance which is not attributable to Faradaic processes.

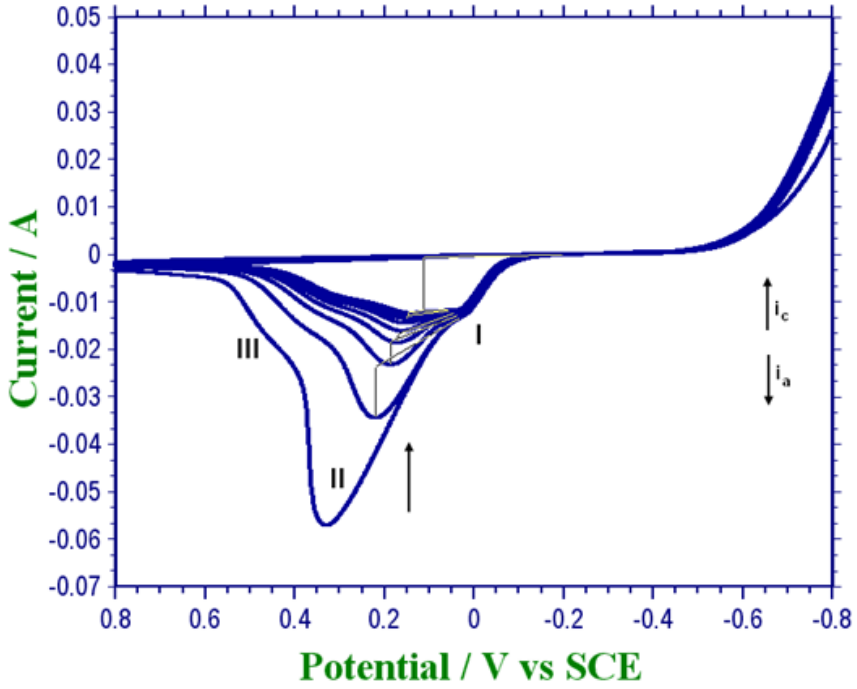


Figure 1. Multicycle CV scans of Nickel electrode in 0.1 M H_2SO_4 solution at 50 mV/s scan rate.

Electrochemical experiments have demonstrated that the activation and passivation reactions at different potentials involve reduction of H_2SO_4 and the production and dissolution of nickel salt, respectively, which is known as the oscillation process (17).

Downloaded on 2017-10-16 to IP 54.70.40.11 address. Redistribution subject to ECS terms of use (see ecsdl.org/site/terms_use) unless CC License in place (see abstract).

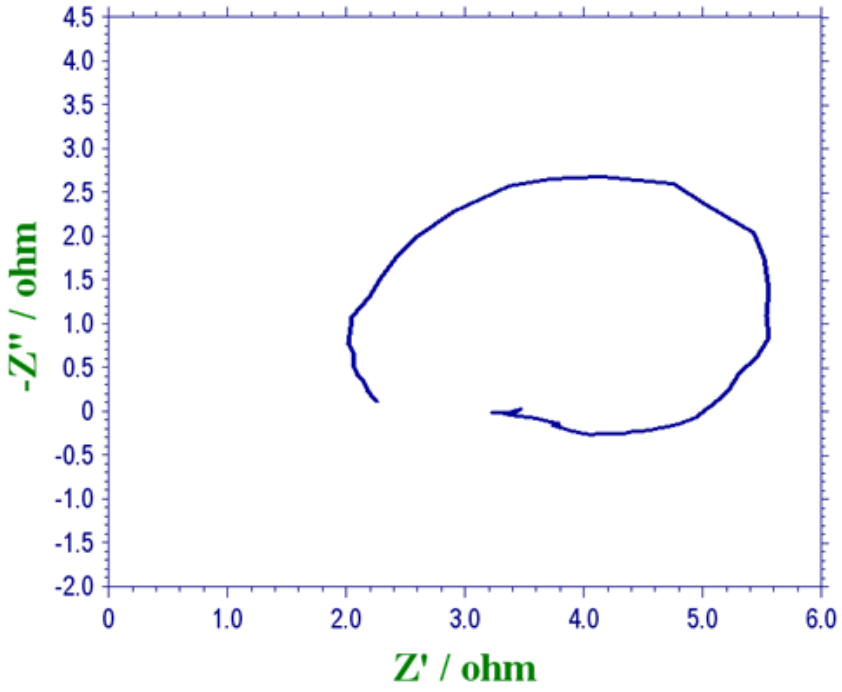


Figure 2. Nyquist diagram of Nickel electrode in 0.1M H_2SO_4 solution after potentiodynamic polarization

Behavior of the Nickel electrode in acidic peroxide solution

The CV graphs of nickel electrode in Figure 3 are given in order to clarify the anodic behavior of nickel in solutions with and without peroxide. It is observed that the addition of H_2O_2 into the acidic solution changes the potentiodynamic behavior of Ni significantly. The current of the peak at 0.15 V is unchanged due to formation of a Ni salt (NiS) and the peak at 0 V is attributed to the formation of $(NiOH)_{ads.}$

The irreversible behavior of Nickel in acidic solution is observed to change with the addition of peroxide. It is known that hydrogen peroxide can be reduced on the metal electrode surfaces. The mechanism for H_2O_2 electrochemical reduction on metal surfaces appears to proceed through the adsorption of a hydroxide radical (13). In the presence of H_2O_2, the cathodic reaction is as follow;

$$H_2O_2 + 2e^- \rightarrow 2OH^- \quad [11]$$

$$H_2O_2 + e^- \rightarrow OH^* + OH^- \quad [12]$$

Moreover, the overall reduction water-peroxide couple takes place in the acidic media according to the following reaction [13].

$$H_2O_2 + 2e^- + 2H^+ \rightarrow 2H_2O \quad [13]$$

$$HO_2^- + 2e^- + H_2O \rightarrow 3OH^- \quad [14]$$

The hydroxide ions formed in the solution are adsorbed on the surface solvated with water. Figure 4 shows the multicycle cyclic voltammogram of nickel electrode in 0.1 M

Downloaded on 2017-10-16 to IP 54.70.40.11 address. Redistribution subject to ECS terms of use (see ecsdl.org/site/terms_use) unless CC License in place (see abstract).

H_2SO_4 + 1M, 1 ml H_2O_2 solution at a scan rate of 50 mV/s. The addition of peroxide results the appearance of a peak at -0.45 V which was attributed to the oxidation of H_2O_2 as mentioned by [13].

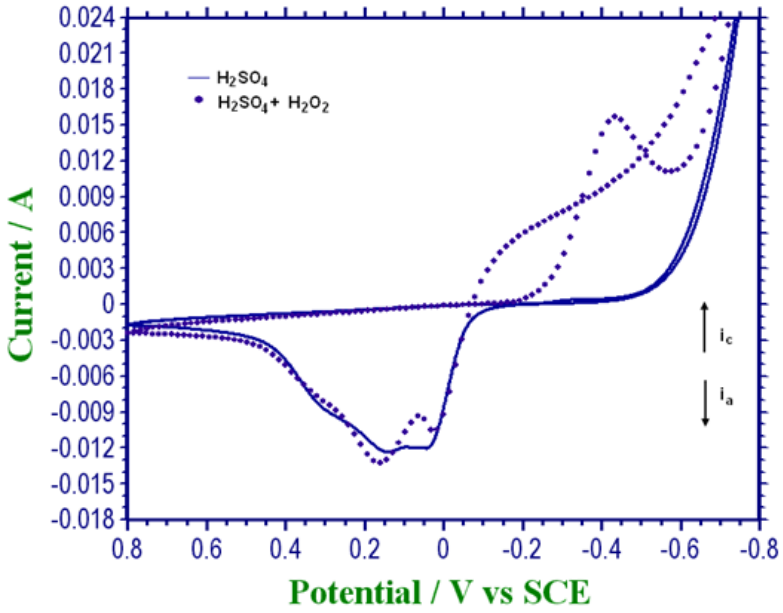


Figure 3. Comparison of CV graphs of Nickel electrode in 0.1M (—) H_2SO_4 and (●) 0.1 M 10ml H_2SO_4+1M, 1 ml H_2O_2 solutions

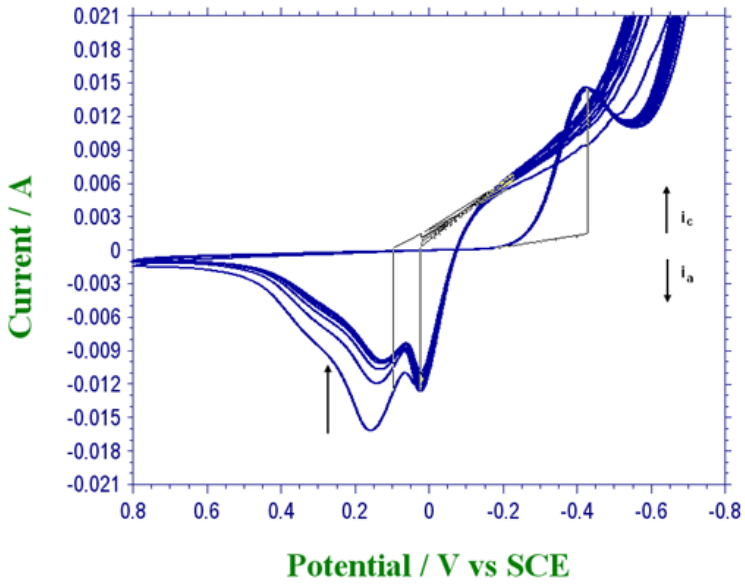


Figure 4. Multicycle in 0.1 M 10 ml H_2SO_4 + 1M, 1 ml H_2O_2 solution of Nickel electrode at a scan rate of 50 mV/s.

Figure 5 shows the CV curves of nickel electrode with various H_2O_2 concentrations. The facts observed in the CV graphs can be summarized as follows:

i. The anodic reaction current at 0.15 V remains unchanged with the addition of H_2O_2. It was verified that at that potential sulphuric acid oxidizes to S^{-2} forming layers of

Downloaded on 2017-10-16 to IP 54.70.40.11 address. Redistribution subject to ECS terms of use (see ecsdl.org/site/terms_use) unless CC License in place (see abstract).

Ni salt on the electrode. It was observed that there was no new peak formation in the anodic region with the addition of peroxide. This is attributed to the hindrance of H_2O_2 oxidation process on Ni electrode (18).

ii. The peak attributed to the $(NiOH)_{ads}$ at 0.0 V is observed at low peroxide concentrations (addition of 1 ml peroxide) and disappears with the addition of further peroxide. This was attributed to the cleavage of this adsorbed layer upon the addition of peroxide.

iii. A cathodic peak appears at -0.45 V upon the addition of peroxide. The addition of further peroxide increases the cathodic current, implying a catalytic activation under higher peroxide concentrations. It is known that NiO is formed on the electrode surface when Ni is exposed to peroxide solution (12). The cathodic current detected at -0.45 V corresponds to the oxidation of nickel to NiO based on the following reactions:

$$Ni + 2OH^- \rightarrow NiO + H_2O + 2e^- \quad [15]$$

$$Ni(III) + e^- \leftrightarrow Ni(II) \quad [16]$$

However, the decrease in the resistance of the surface causes the increase of the cathodic reaction current and the electrode surface is activated due to the dissolution mechanism of the NiO as follows (19):

$$NiO(s) \leftrightarrow Ni^{+2}(l) + O^{-2}(l) \quad [17]$$

iv. The peak observed at 0.35 V in peroxide-free solution is also present after the addition of peroxide. It is attributed to formation of Nickel oxyhydroxide (NiOOH).

The results indicate that Ni shows passivation behavior in the anodic region and activation behavior in the cathodic region in the peroxide solution with H_2SO_4. Nyquist diagrams (Figure 6) clearly reveal the passivation and activations states that will be discussed in the following section.

Downloaded on 2017-10-16 to IP 54.70.40.11 address. Redistribution subject to ECS terms of use (see ecsdl.org/site/terms_use) unless CC License in place (see abstract).

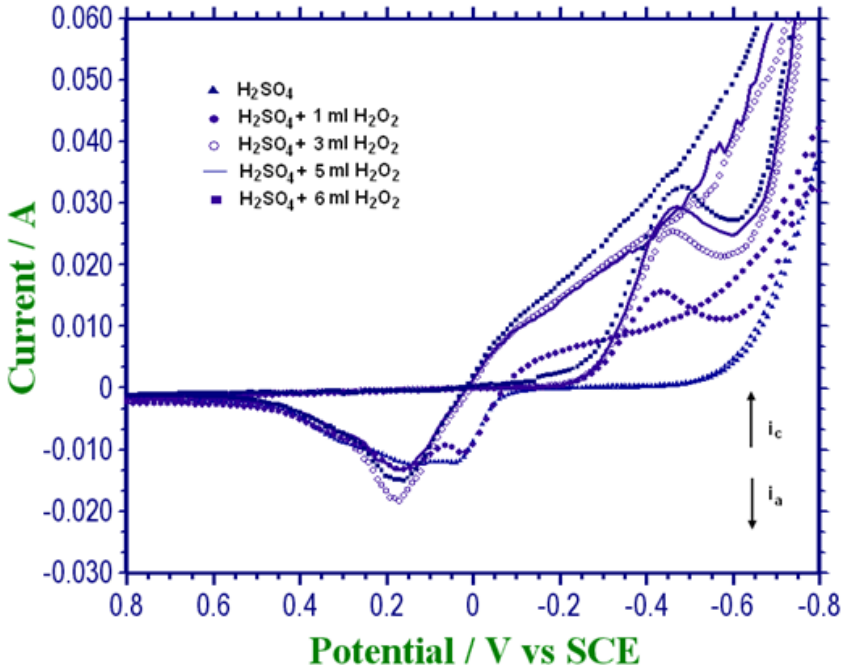


Figure 5. Comparison of CV graphs of Nickel electrode in 0.1 M H_2SO_4 solution and with addition of different concentrations of 1 M H_2O_2 solution

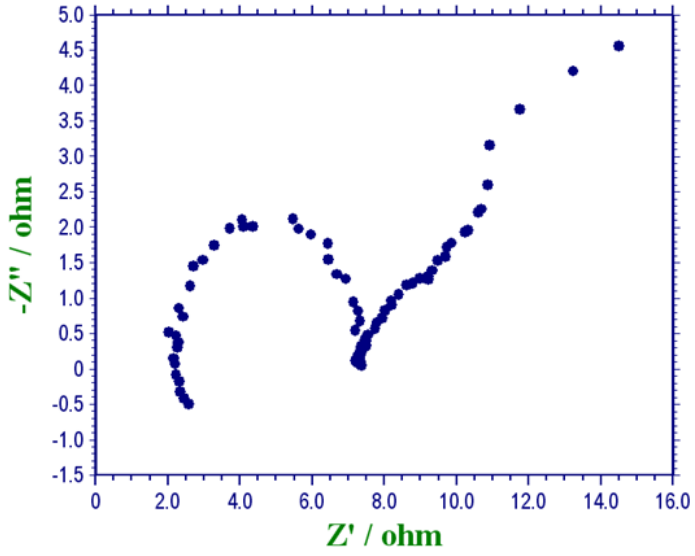


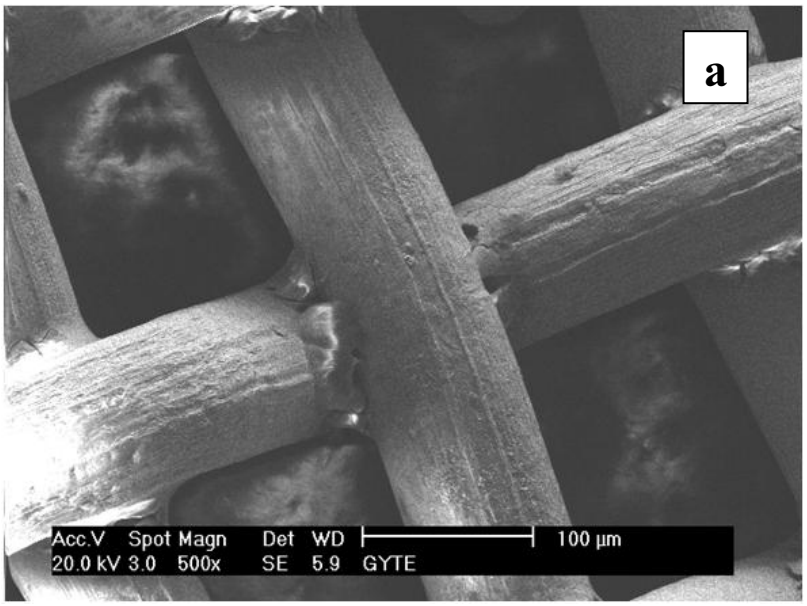
Figure 6. The Nyquist diagram of Nickel in the acidic solution with addition of 1 M, 1 ml of peroxide

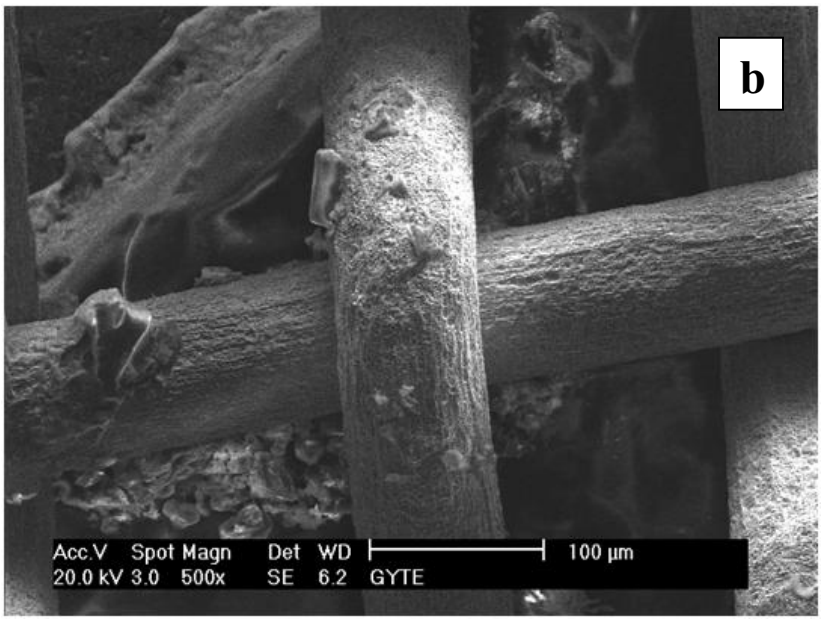
Physical characterization of Ni surface

The modern characterization techniques, such as scanning Electron microscopy (SEM) and Energy-dispersive X-ray spectroscopy (EDAX), were used for determination of the surface topography and for compositional analysis, respectively. Figure.7 shows the surface of the untreated Ni electrode (Figure 7a), and the Ni electrode treated with H_2SO_4 (Figure 7b) and H_2SO_4+H_2O_2 (Figure 7c). The morphological features of the

Downloaded on 2017-10-16 to IP 54.70.40.11 address. Redistribution subject to ECS terms of use (see ecsdl.org/site/terms_use) unless CC License in place (see abstract).

Figure 7a,b and c are different . The comparison of Figure 7a and Figure 7b shows that the surface exposed to H_2SO_4 is rougher than that of the untreated Ni surface. In Figure 7b, most particles have been agglomerated in the corner of Ni net but in Fig 7c the particles are separated from each other and particles sizes are bigger than those observed on H_2SO_4 treated surface. The SEM images provided a further data on the surface roughness caused by the dissolution of Ni in H_2SO_4 and H_2SO_4+H_2O_2 solutions. EDAX measurements were employed to investigate the local surface structure and composition of Ni surface covered with oxide, hydroxide and salt. However the chemical nature of hydroxylation (bulk $Ni(OH)_2$ or hydrated NiO) is not clear even with EDAX analysis.





Downloaded on 2017-10-16 to IP 54.70.40.11 address. Redistribution subject to ECS terms of use (see ecsdl.org/site/terms_use) unless CC License in place (see abstract).

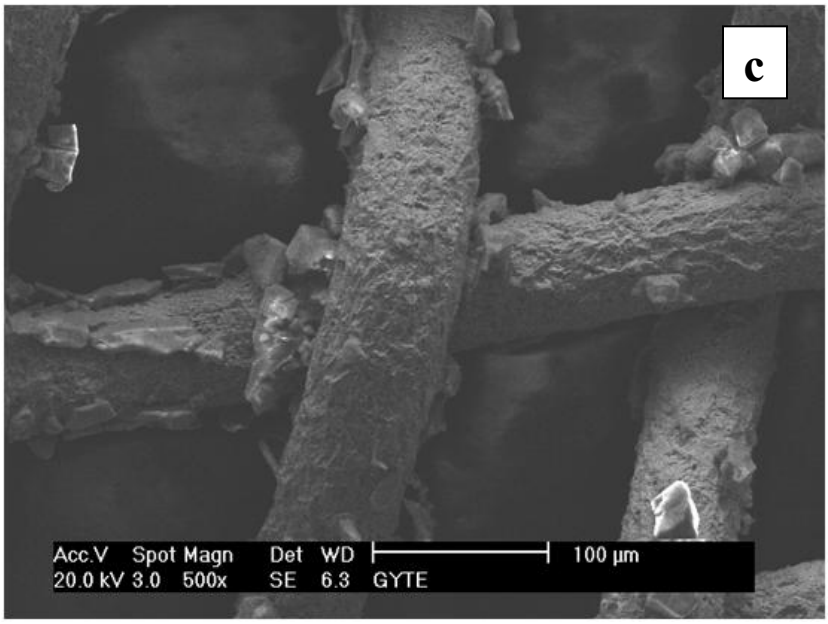


Figure 7. The SEM images of the Ni surface **a)** untreated, **b)** treated with H_2SO_4 and **c)** treated with H_2SO_4 + H_2O_2 solutions.

The EDAX profile of the untreated Nickel given as an insert in Figure 7a shows the peaks belonging to pure Ni. Figure 8 the SEM image and the EDAX results of the selected areas marked with circles in Figure 8 are presented. As seen from Figure 8 the sizes of the particles formed on the electrode surface are not homogeneously distributed. According to the EDAX analysis the Nickel peak was detected in the area.1. However the structures formed on the surface marked as point 1 and point 2 contain the sulphur and oxide as expected. It is anticipated that H_2SO_4 reduces to S^{-2} species as a Ni salt on the electrode surface according to Eq 8**.** On the other hand, a Nickel oxide layer (NiOOH) and S^{-2} simultaneously formed on the surface at more positive potentials. However, the amount and chemical nature of oxide and hydroxide structures ($Ni(OH)_2$, NiOOH or NiO) could not be not clarified by EDAX analysis.

Downloaded on 2017-10-16 to IP 54.70.40.11 address. Redistribution subject to ECS terms of use (see ecsdl.org/site/terms_use) unless CC License in place (see abstract).

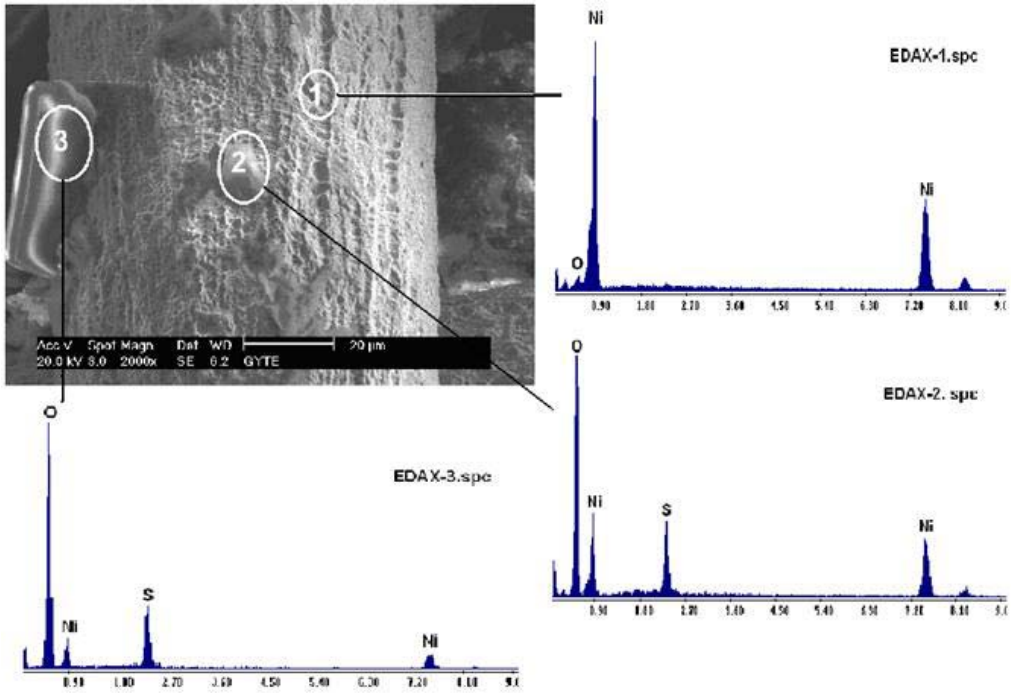


Figure 8. The SEM image, and EDAX results taken from certain areas for Ni surface treated with H_2SO_4 solution.

The SEM image and EDAX patterns of the Ni surface treated with H_2SO_4 + H_2O_2 solution are given in Figure 9. There is a remarkable difference in the SEM images of the Ni surface between two surfaces treated with peroxide and peroxide free acidic solutions. At point 1 in Figure 9, there are sulphur and oxide peaks in acidic peroxide solution, while there is only the Nickel peak in peroxide free acidic solution. Although the electrode seems to be deactivated in peroxide free acidic solution the addition of peroxide causes an appearance of a peak at -0.50 V in the cathodic scan corresponding to the reduction of peroxide. This peak increases with the increasing peroxide concentration. There was not a significant change in the anodic scan (Figure 5). This peak increases with the increasing peroxide concentration. The opening loop of the Nyguist graph (Figure 6). Although there is no cathodic peak for Ni electrode in peroxide free H_2SO_4 solution there appears a cathodic peak which increases with the increase in increasing peroxide concentration which is attributed to the reduction of peroxide (Figure 6). From CV results and the literature that a NiO layer forms on the surface which supplies the electrons during the anodic reduction according to Eq.16 (12).

Downloaded on 2017-10-16 to IP 54.70.40.11 address. Redistribution subject to ECS terms of use (see ecsdl.org/site/terms_use) unless CC License in place (see abstract).

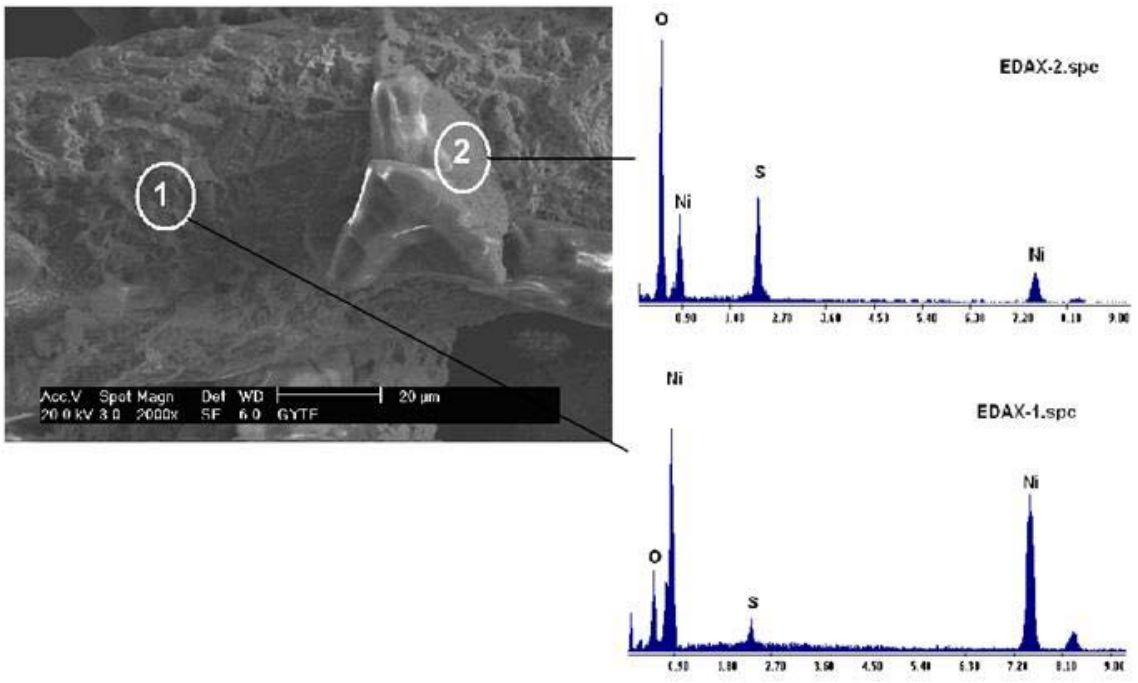


Figure 9. The SEM image and EDAX results taken from certain areas for Ni surface treated with $H_2SO_4 + H_2O_2$

Electrochemical Impedance Spectroscopy study

The electrochemical impedance is a powerful method for the detailed mechanistic analysis. Impedance models can be classified as process models and measurement models [20]. Process models are based on the mathematical description of physical phenomena and therefore incorporate physically meaningful parameters which can be identified by measurement and optimization. In contrast, measurement models are mathematical structures with shapes that fit to measured impedance spectra. Electrochemical models may have a large number of parameters (charge-transfer resistance, reaction rate coefficients, diffusion coefficients), and simulated impedance properties (relaxation frequency, polarization resistance) and they do not show a simple dependence on a single parameter.

The simulated impedance reflects the physicochemical properties of the assumed electrochemical reaction model. If the experimental data are available, model parameters can be estimated by varying their values until a best agreement between simulation results and experimental data is obtained (fitting).

The basic elements for describing impedances are ohmic resistance R_Ω, capacitance C, inductance L and Warburg impedance W: $Z_R=R$, $Z_C=(j\omega C)^{-1}$, $Z_L=j\omega L$ and $Z_W=(j\omega W)^{0.5}$. If the membrane/electrode interface and catalyst layer have the structures of quite porous and rough, it cannot be simulated as ideal capacitors. The constant phase element (CPE) is required to simulate such non-ideal conditions. The impedance of CPE is expressed as: $Z=[Q(j\omega)^p]^{-1}$ $(0.5 < p < 1.0)$ (20).

Downloaded on 2017-10-16 to IP 54.70.40.11 address. Redistribution subject to ECS terms of use (see ecsdl.org/site/terms_use) unless CC License in place (see abstract).

Impedance model of Nickel in H_2SO_4 solution

The task of modeling the impedance is to find an equivalent circuit which shows the identical electrical behavior and derive a mathematical expression which reflects the essential properties of the electrochemical system. The theoretical impedance analysis of the anodic dissolution of nickel was investigated by Gregori (21).

i. Fitting of simulated impedance spectra to experimental data

Figure 11 depicts the electrochemical impedance spectra and the simulated Nyquist plot for Nickel electrode in H_2SO_4 solution. It can be seen from the corresponding Nyquist diagram, the impedance response of the Ni electrode in H_2SO_4 solution is characterized by the presence of a depressed semicircle caused by the passive layers such as NiS and NiOOH formed on the electrode surface and an inductive behavior indicating that the charge transfer resistance was dominant. The electrolyte resistance R_Ω was determined at high frequencies. In case of Ni/Ni^{+2} dissolution reaction controlled by a charge transfer process the impedance of the reaction is simply presented R_{ct} connected with C_{dl}. At lower frequency region an inductive effect was observed which indicated mass transfer effects.

According to Figure 10 the total impedance can be obtained as follows:

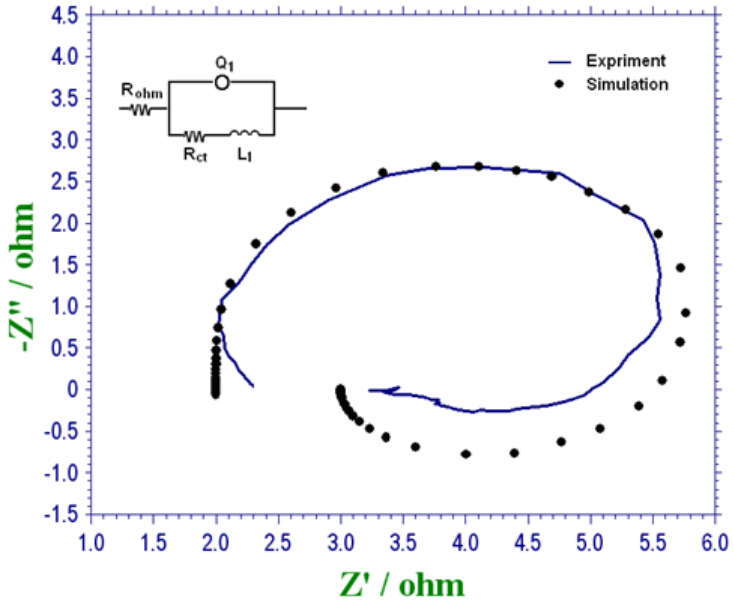


Figure 10. Nyquist diagram and equivalent circuit of Nickel electrode in 0.1 M H_2SO_4 solution.

$$Z_{Total} = R_\Omega + \frac{1}{\frac{1}{Z_{CPE}} + \frac{1}{Z_{Rct} + Z_L}} = R_\Omega + \frac{j\omega L + R_{ct}}{j^2\omega^2 LC + j\omega\tau_1} \qquad (18)$$

Downloaded on 2017-10-16 to IP 54.70.40.11 address. Redistribution subject to ECS terms of use (see ecsdl.org/site/terms_use) unless CC License in place (see abstract).

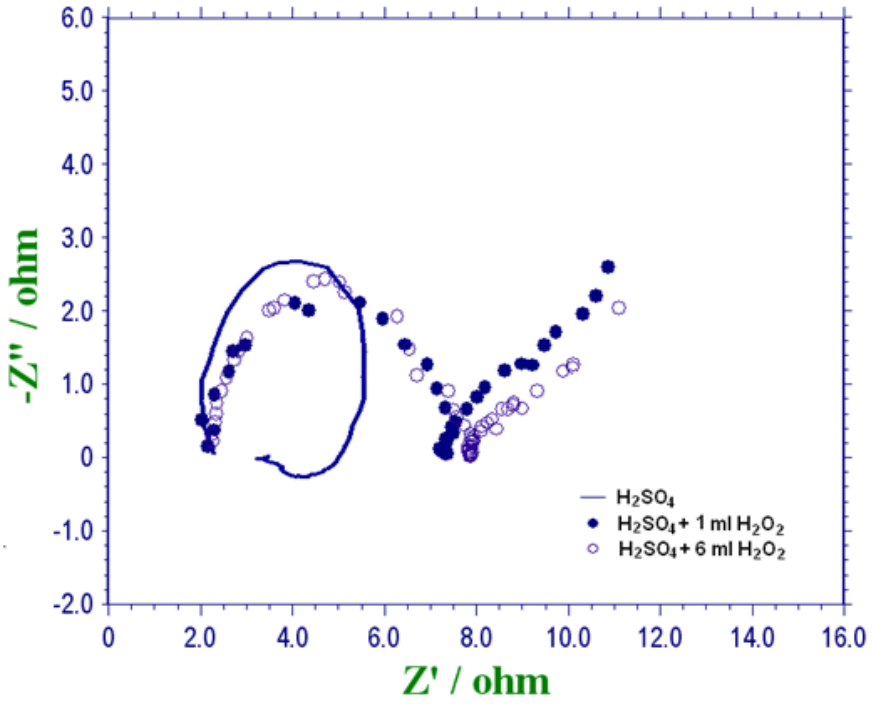


Figure 11. Nyquist diagrams of Nickel in (—) H_2SO_4, (●) H_2SO_4+ addition of 1 ml 0.5 M H_2O_2 and (○) H_2SO_4+ addition of 6 ml 0.5 M H_2O_2 solutions

There is a good agreement between the fitted and experimental curves as seen Figure 10. The impedance parameters are tabulated in Table.1.

ii. The process model of Ni in H_2SO_4 solution by EIS

This approach can directly yield values of physical and chemical properties of the system (rate coefficients, exchange current densities, diffusion coefficients, and details about the reaction mechanisms itself) (22).

The impedance plot shown in Figure 11 consists of a loop reflecting an inductive behavior. The impedance behavior was explained using the kinetic theory for reaction involving intermediate adsorbed or covered on the electrode surface [22]. It is known that following irreversible mechanisms is dominant on Ni surface in the H_2SO_4 solution which was also verified by multi-cycle CV graphs (Figure 1):

$$Ni \rightarrow Ni^{+2} + 2e^{-} \qquad E^{0} = 0{,}23\ V \qquad (19)$$

Bard proposed the following expression for the irreversible systems to calculate the reaction rate constant [23]. This equation gives an approximation between the rate constant and peak potential/current (I_p, E_P) in practical CV applications. The reaction rate constant of the Nickel in the 0.1 M H_2SO_4 solution can be found by the use of I_p/E_p values calculated from Figure 1.

Downloaded on 2017-10-16 to IP 54.70.40.11 address. Redistribution subject to ECS terms of use (see ecsdl.org/site/terms_use) unless CC License in place (see abstract).

$$i_p = 0{,}227.n.F.A.C_0^*.k^0 \exp\left(-\left(\frac{\alpha n_a F}{RT}\right)\left(E_p - E^0\right)\right) \quad (20)$$

$$3.926\times10^{-3} = 0.227\times2\times96500\times0.1068\times k_0 \times \exp\left[-\left[\frac{0.5\times2\times96500}{8.314\times298}\right](0.116)\right]$$

The major aim of this study is to make a comparison between the rate constants calculated by CV and EIS. The rate constant was calculated by EIS using the following expression derived by Barsukov (20).

$$R_{ct} = \frac{RT}{n^2F^2k(C_{OH^-})^{\alpha}(C_{H^{+3}O})^{1-\alpha}} \quad (21)$$

The parameter of the charge transfer resistance R_{ct} given in Table.1 was used in the equation. Assuming that the concentrations of $C_{H^{+3}O}$ and C_{OH^-} produced by the oxidation reactions are the equal, the expression can be simplified and rate constant can be calculated as follows:

$$9.363 = \frac{8{,}314\times298}{2^2\times96500^2\times k_0\times\left(0.1\times10^{-3}\right)}$$

Table.2. list the kinetic parameters by the use of two different models. It is seen that the results found by the two methods are in good agreement.

TABLE I. Calculation of the impedance parameters

	R_{ohm} ohm	Q_1 ohm^{-1}	R_{ct} ohm	W $ohm.sn^{1/2}$	Q_2 ohm^{-1}	R_2 ohm
H_2SO_4	2	4.3e-5	1			
H_2SO_4 + 2 ml H_2O_2	2	0.168 n=0,9	1	0.65	1.2e-4 n=0.85	5.5
H_2SO_4 + 6 ml H_2O_2	2.2	0.22 n=0.98	0.9	0.95	2e-4 n=0.89	5.7

Downloaded on 2017-10-16 to IP 54.70.40.11 address. Redistribution subject to ECS terms of use (see ecsdl.org/site/terms_use) unless CC License in place (see abstract).

TABLE II. The values used for calculation of the rate constant of the Ni electrode in the H_2SO_4 solution

i_p	3.928×10^{-3} A	
E_p	-0.114 V (SHE)	
E_0	-0.23 V (SHE)	
n	2	
F	96500 C/mol	
α	0.5	
C_0^*	$0.1x10^{-3}$ mol/cm^3	
R	8.314 J/mol.K	
A	0.1068 cm^2	
k_0	**7.69×10^{-5} cm.sec^{-1}**	**(CV)**
	7.1×10^{-5} cm.sec^{-1}	**(EIS)**

The impedance model of Ni in H_2SO_4+ H_2O_2 solution

The impedance behavior of Ni exposed to H_2SO_4 + H_2O_2 mixed solution differs from that of the Nickel in H_2SO_4 (Figure 12). There appears a line at low frequencies with an angle of 45^0 to the real axis. This type of behavior is explained by the Warburg impedance (Z_W). In this case, the system is under diffusion control and the surface has active sides for the reduction of peroxide. On the other hand, it is known that the formation Ni salts and Ni oxides on the surface with the presence of H_2SO_4 deactivate the surface (Figure 9 and Figure 11). The activation effect of the peroxide solution is clearly seen from Figure.11 verified by the presence of Warburg impedance.

i. Fitting of simulated impedance spectra to experimental data

The impedance spectra, simulated curves and equivalent circuits of the Ni in the H_2SO_4 + 1 ml H_2O_2 and H_2SO_4+ 6 ml H_2O_2 are shown in Figure 12 and Figure 13 There is a very big difference between two Nyquist diagrams. Impedance parameters were obtained by fitting the data to an equivalent circuit. The circuit elements are explained as follows. R_{ct} and Q_1 are the resistance corresponding to the charge transfer resistance of NiS and NiOOH formed on Nickel surface and constant phase element due to distribution of microscopic material properties, respectively, in mid-frequency range. The second relaxation process (R_2 and Q_2) associated with Warburg impedance which exhibits the diffusion process appeared at low frequencies. The impedance parameters measured by the fitting process are listed in Table 1.

Downloaded on 2017-10-16 to IP 54.70.40.11 address. Redistribution subject to ECS terms of use (see ecsdl.org/site/terms_use) unless CC License in place (see abstract).

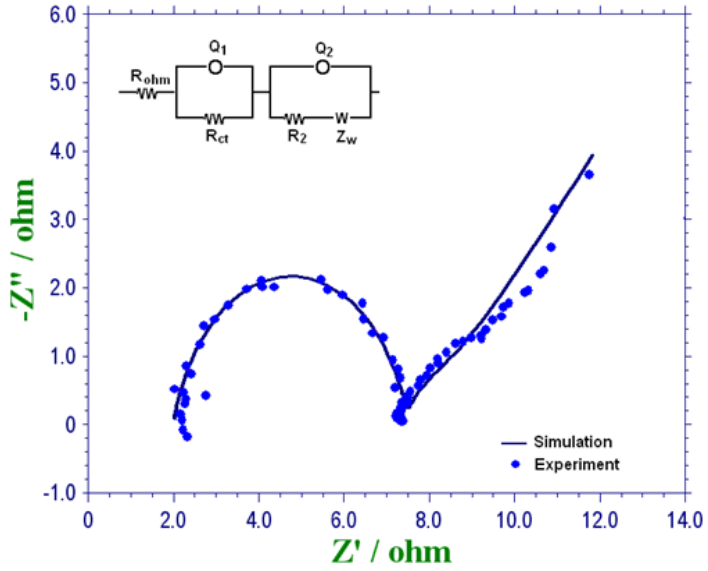


Figure 12. Nyquist diagram of Nickel electrode in H_2SO_4 + 1 ml of H_2O_2, experimental (●) and simulation (—) curves

$$Z = R_{ohm} + \frac{1}{\frac{1}{Z_{CPE}} + \frac{1}{R_{ct}}} + \frac{1}{\frac{1}{Z_{CPE}} + \frac{1}{R_2} + \frac{1}{Z_W}}$$

$$= R_{ohm} + \frac{R_{ct}}{Q(j\omega)^n R_{ct} + 1} + \frac{R_2 (j\omega W)^{0.5}}{(Q(j\omega)^n R_2 + 1) \times (j\omega W)^{0.5} + R_2} \qquad (22)$$

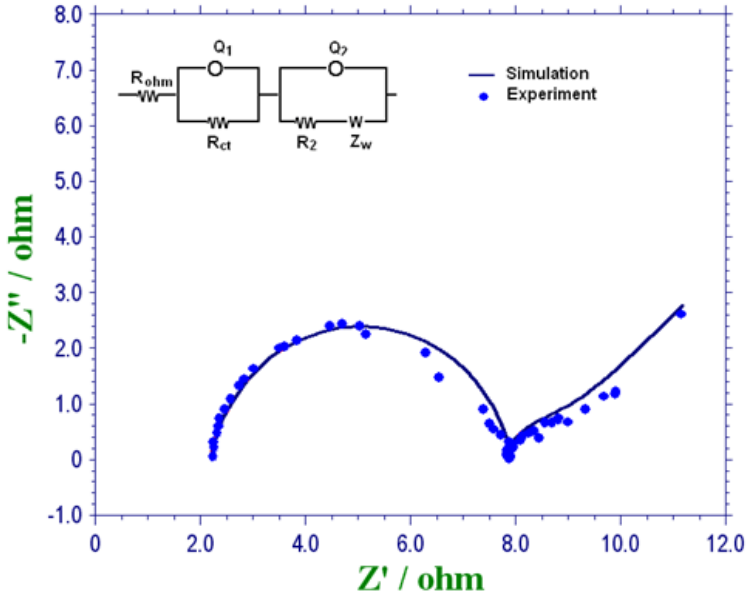


Figure 13. Nyquist diagram of Nickel electrode in H_2SO_4 + 6 ml of H_2O_2, experimental (●) and simulation (—) curves

Downloaded on 2017-10-16 to IP 54.70.40.11 address. Redistribution subject to ECS terms of use (see ecsdl.org/site/terms_use) unless CC License in place (see abstract).

ii. The process model of Ni in H_2SO_4+H_2O_2 solution by EIS

Similarly, two impedance models were developed for acidic peroxide condition. Since this system is irreversible and diffusion controlled as seen from the CV plots the following expression proposed by Bard can be used to calculate the diffusion coefficient (D_A) (23). The values used in the equation and the diffusion coefficient measured are tabulated in Table.3.

$$i_p = 2.99\times10^5 \times \alpha^{1/2} \times A \times D_0^{1/2} \times C_0^* \times \nu^{1/2} \quad (23)$$

The diffusion coefficient can also be calculated from the EIS data by the use of following formula derived by Barsukov (20);

$$W = \sigma\omega^{-1/2} - j\sigma\omega^{-1/2} \quad (24)$$

$$\sigma = \frac{RT}{n^2F^2A\sqrt{2}}\left[\frac{1}{C_{H2O2}(D_{H2O2})^{1/2}} + \frac{1}{C_{Product}(D_{Product})^{1/2}}\right] \quad (25)$$

If Q_1 is small the imaginary part of W, Im(W) and $\omega^{1/2}$ can be assumed to be equal to σ at all frequencies [20]. Since the Q_1 is very small from Table.1, as a general approach this assumption is acceptable. So σ was estimated from the value of Warburg impedance given in Table.1.

$$W = \sigma \times \sigma^{-1} - \sigma = 1 - \sigma$$
$$W = 0.65 \quad \text{ohm.sec}^{-1/2}$$
$$\sigma = 0.35 \quad \text{ohm.sec}^{-1/2}$$

On the other hand taking $\frac{1}{C_{Product}(D_{Product})^{1/2}} << \frac{1}{C_{H_2O_2}(D_{H_2O_2})^{1/2}}$ into consideration in the final expression the diffusion coefficient can easily be calculated from the Barsukov Eq.25 (20). The related values and diffusion coefficients calculated by the use of two different methods are given in Table 3.

TABLE III. The values used for calculation of the diffusion coefficient of Ni electrode in the H_2SO_4+H_2O_2 solution

i_p	1.374×10^{-2} A	
n	1	
F	96500	
A	0.08 cm^2	
C_0^*	$0.09\text{x}10^{-3}$ mol/cm^3	
γ (scan rate)	0.05 V/sn	
D_{H2O2}	**5.43×10^{-3} $cm^2.sec^{-1}$**	**(CV)**
	5.57×10^{-3} $cm^2.sec^{-1}$	**(EIS)**

Downloaded on 2017-10-16 to IP 54.70.40.11 address. Redistribution subject to ECS terms of use (see ecsdl.org/site/terms_use) unless CC License in place (see abstract).

It is observed from CV graphs (Figure 4-5) that the peroxide could be reduced on the Nickel surface and the cathodic current increases with the increasing peroxide concentration. The Nyquist diagrams confirmed the CV results that surface was activated.

It is observed from the cyclic voltammograms of Ni that H_2SO_4 is oxidized in the anodic scan and peroxide is reduced in the cathodic scan. Both reactions take place in an irreversible way. Therefore the equations given for the irreversible reactions can be employed without any problem. The parameters obtained by the use of CV and EIS techniques were observed to in good accordance.

Conclusions

Consequently, the conclusions can be summarized as follow:

i. It is clearly seen that nickel surface deactivated in the sulphuric acid with formation of the passive layers can be activated by addition of the peroxide solution. According to the EIS results the Warburg impedance revealed in the acidic peroxide solution. Moreover activation of the electrode surface was verified by CV graphs.

ii. The hydrogen peroxide reduced to the water instead of the oxygen on the nickel electrode in the acidic peroxide solution. It is indicated that Nickel can be used as the cathode catalyst in the fuel cells instead of the platinum which causes the formation of the oxygen, an undesired reaction, by a chemical mechanism. The performance tests of a passive direct borohydride/peroxide fuel cell constructed with Nickel cathode will be given in the further research as the Part II.

iii. There was dissolution of the Ni electrode observed. This was prevented by coating the metal surface with Nafion.

iv. The surface of the Ni electrode is deactivated in sulfuric by the formation of sulfur salt and oxide layers in an irreversible manner.

v. However the addition of peroxide reactivates the surface observed as the change of impedance parameters and the appearance of Warburg impedance. There is a formation of a cathodic peak at -0.5 V which corresponds to the reduction of the peroxide.

vi. Peroxide is reduced directly to water rather than to hydrogen and oxygen on nickel surface. This one of the prime requirements in direct borohydride / peroxide fuel cells. This shows that nickel can conveniently be used as a cathode material in fuels cell in place of Pt. The investigation of the performance of such a cell is a subject of a future study.

Ni appears to be subjected to a dissolution process in acidic media. This was prevented by covering the electrode with nafion.

Downloaded on 2017-10-16 to IP 54.70.40.11 address. Redistribution subject to ECS terms of use (see ecsdl.org/site/terms_use) unless CC License in place (see abstract).

Acknowledgment

We would like to acknowledge Gebze High Technology Institute for SEM micrographs and EDAX patterns.

References

1. George H. Miley, Nie Luoa, Joseph Mather, Rodney Burton, Glenn Hawkins, Lifeng Gua, Ethan Byrd, Richard Gimlin, Prajakti Joshi Shrestha, Gabriel Benavides, Julia Laystrom, David Carroll, ***J. Power Sources*** 165 (2007) 509–516.
2. R.K. Raman, S.K. Prashant, A.K. Shukla; ***J.f Power Sources*** 162 (2006) 1073–1076.
3. C. Ponce de Le´on, F.C. Walsh, A. Rose, J.B. Lakeman, D.J. Browning, R.W. Reeve, ***J.Power Sources*** 164 (2007) 441–448.
4. E. Sanli, H. Çelikkan, M.L. Aksu, B. Z. Uysal; ***Int. J. Hydrogen Energy***, 33 (2008) 2097-2104.
5. E. Sanlı, H.Çelikkan, M.Levent Aksu, B.Zühtü Uysal, ***ECS Trans*** 5 (2007) 137-145.
6. Marian Chatenet, Fabrice Micoud, Ivan Roche, Eric Chainet; ***Electrochimica Acta*** 51 (2006) 5459–5467.
7. N.Bussayajarn, D.A.Harrington, S.Therdthianwong, A.Therdthianwong, N.Djilali, 30TH Congress On Science & Technology of Thailand, 30:1, (2004).
8. C.P. Leon, F.C.Walsh, A.Rose, J.B. Lakeman, D. J.Browing, R.W.Reeve, ***J. Power Sources***, 155: 172-181, (2006).
9. Dianxue Cao, Jundang Chao, Limei Sun, Guiling Wang, ***J. Power Sources*** 179 (2008) 87–91.
10. G. Selvarani a, S.K. Prashant a, A.K. Sahu a, P. Sridhar a, S. Pitchumani a, A.K. Shukla; ***J. Power Sources*** 178 (2008) 86–91.
11. Lifeng Gu, Nie Luo, George H. Miley, ***J. Power Sources*** 173 (2007) 77–85.
12. Tianbao Du, Arun Vijayakumar, Kalpathy B. Sundaram, Vimal Desai; ***Microelectronic Engineering*** 75 (2004) 234–241.
13. Daniel N. Prater, John J. Rusek, ***6th European space power conference***, Porto, Portugal, May 2002, Vol. 502, pp 705-709, 2002.
14. J.Scherer, B.M. Ocko, O.M. Magnussen, ***Electrochim. Acta*** 48 (2003) 1169-1191.
15. M. Abdallah, A.Y. El-Etre, ***Portugaliae Electrochimica Acta 21 (2003) 315-326.***
16. M.R.F. Hurtado, P.T.A. Sumodjo, A.V. Benedetti; ***Electrochimica Acta*** 48 (2003) 2791-/2798.
17. Yanxu Li, M.B. Ives, K.S. Coley, ***Corrosion Science*** 48 (2006) 1560–1570.
18. R. Kothandaraman, *PhD. Thesis, Faculty of Science, Indian Institute of Science,* May 2006, Bangalore, India.
19. Bo Huang, Gang Chen, Fei Li, Qing-chun Yu, Ke-ao Hu, ***Electrochim. Acta*** 49 (2004) 5055-5068.
20. Evgenij Barsoukov, J.Ross Macdonald, Impedance Spectroscopy Theory, experiment and Application, Second edition, John Wiley&Sons (2005), pp. 20-26.
21. A.J.Bard, L.R.Faulkner, "Electrochemical methods, fundamentals and applications", Second Edition, ***John Wiley&Sons***, (2001) pp. 236.

Downloaded on 2017-10-16 to IP 54.70.40.11 address. Redistribution subject to ECS terms of use (see ecsdl.org/site/terms_use) unless CC License in place (see abstract).